Development and application of a predictive fermentation model for continuous and pressurized fermentation using Clostridium ljungdahlii

Christian F.W. Ebel, Lukas Richter, Steven Minden, Thomas Meurer, Anne-Kristin Kaster, Moritz Wolf, Jörg Sauer

PII: S1385-8947(25)12591-6

DOI: https://doi.org/10.1016/j.cej.2025.171744

Reference: CEJ 171744

To appear in:

Received date: 30 July 2025

Revised date: 8 November 2025

Accepted date: 8 December 2025

Please cite this article as: C.F.W. Ebel, L. Richter, S. Minden, et al., Development and application of a predictive fermentation model for continuous and pressurized fermentation using Clostridium ljungdahlii, (2024), https://doi.org/10.1016/j.cej.2025.171744

Development and Application of a Predictive Fermentation Model for Continuous and Pressurized Fermentation Using *Clostridium ljungdahlii*

Christian F. W. Ebel[a], Lukas Richter[b], Steven Minden[c], Thomas Meurer[b], Anne-Kristin Kaster[c,d], Moritz Wolf[a,e], Jörg Sauer[a,*]

a Institute of Catalysis Research and Technology (IKFT), Karlsruhe Institute of Technology (KIT), Eggenstein-Leopoldshafen/ Germany

b Institute of Mechanical Process Engineering and Mechanics (MVM), Karlsruhe Institute of Technology (KIT), Karlsruhe/ Germany

c Institute for Biological Interfaces (IBG-5), Karlsruhe Institute of Technology (KIT), Eggenstein-Leopoldshafen/ Germany

d Institute of Applied Biosciences (IAB), Karlsruhe Institute of Technology (KIT), Karlsruhe/ Germany

e Engler-Bunte-Institut (EBI), Karlsruhe Institute of Technology (KIT), Karlsruhe/ Germany

*Corresponding author: j.sauer@kit.edu

Graphical Abstract:

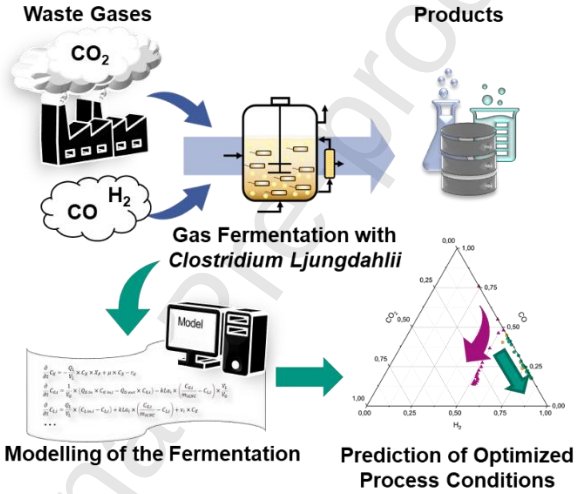

Abstract

Utilization of CO_2-containing industrial waste gas emissions as substrates for fermentation with acetogen bacteria is a novel approach. A key requirement for successful process optimization and the development of advanced control strategies is a robust model that can sufficiently predict system responses to varying process conditions. However, few fermentation models have been developed for continuous cell retention or elevated pressure conditions, which are beneficial for integrating gas fermentation with CO_2 separation technologies. Therefore, this study adapts a dynamic kinetic model to simulate these conditions to enable model-supported process design with *Clostridium ljungdahlii*. The literature model was modified by adjusting key equations and re-estimating important kinetic parameters derived from long-term fermentation experiments in a continuous stirred tank reactor. Addition of a carbon dioxide dependency to the hydrogen uptake rate and the acetate to ethanol conversion rate improves the model's accuracy to predict biomass and product concentration trends under high hydrogen substrate gas and moderately increased pressure conditions. Model predictions indicate that maximum ethanol production is linked with biomass growth and increases more than tenfold when the gas residence time is lowered from 1.80 to 0.09 h, and the H_2 content in the substrate gas is simultaneously raised from 60 to 80%, with the remainder being CO. Maximum acetate production is predicted to increase with lower gas residence time, 50% H_2 in the feedstock gas and a shift from CO to a mixture of CO and CO_2 as a carbon source, with a CO_2 content of up to 30%.

Keywords:

gas fermentation, kinetic model, acetogens, *Clostridium ljungdahlii*, pressure, process optimization

Highlights:

- A model was developed to represent continuous, pressurized conditions
- The addition of CO_2 dependency enhances the model's predictive capability
- The modified model accurately predicts outcomes under moderate pressure conditions
- Substrate gas residence time and composition influence the product spectrum

1. Introduction

In the face of climate change, the capture and use of the waste gas carbon dioxide (CO_2) has become increasingly important. Fossil CO_2 contributes up to 68% of global greenhouse gas emissions [1]. To reduce emissions, it is crucial to optimize existing and new carbon capture and storage (CCS) and utilization (CCU) technologies [2], [3]. One such promising technology is gas fermentation [4], [5]. In this process, acetogenic microorganisms use gas mixtures containing carbon monoxide (CO), CO_2, and hydrogen (H_2) to produce fuels and basic chemicals, such as ethanol, acetic acid, butanol, butyrate, or hexanol [6], [7], [8], [9]. Many anaerobic organisms follow the Wood-Ljungdahl pathway (WLP) under autotrophic conditions [9]. In this pathway, CO or mixtures of CO_2 and H_2 provide a carbon source or a reduction equivalent in the case of H_2 [10]. Ethanol can be produced directly from acetaldehyde, an intermediate product of the WLP, through conversion with aldehyde dehydrogenase (ALDH), followed by reduction with alcohol dehydrogenase (ADH). Alternatively, it can be produced from acetate via conversion with aldehyde ferredoxin oxidoreductase (AOR) and subsequent reduction with ADH [9], [11]. Gas fermentation is already industrially deployed to produce ethanol as a biofuel from steel mill emissions [7], [12], [13]. Higher-value products are achieved with mixed-culture fermentation or sequential co-fermentation [14], [15], [16]. Another promising application for gas fermentation is the integration of this process with other CCS or CCU technologies, such as electrocatalytic CO_2 reduction, for more efficient use of waste gases [17], [18]. *Clostridium ljungdahlii*, an acetogenic, anaerobic, rod-shaped, gram-positive bacterium that primarily produces acetate and ethanol, is commonly cultivated for gas fermentation [19]. Equations 1-6 list the proposed simplified reactions for the production of acetic acid (HAc) and ethanol (EtOH) by this organism.

$$4CO + 2H_2O \rightarrow HAc + 2CO_2 \quad (1)$$
$$4H_2 + 2CO_2 \rightarrow HAc + 2H_2O \quad (2)$$
$$HAc + 2CO + H_2O \rightarrow EtOH + 2CO_2 \quad (3)$$
$$HAc + 2H_2 \rightarrow EtOH + H_2O \quad (4)$$
$$6CO + 3H_2O \rightarrow EtOH + 4CO_2 \quad (5)$$
$$6H_2 + 2CO_2 \rightarrow EtOH + 3H_2O \quad (6)$$

The influence of different process parameters on the fermentation with this organism has been explored in batch and continuous experiments [20], [21], [22], [23], [24], [25], [26]. Liquid solubility of the substrate gases is one of the main limiting factors in gas fermentation and can be increased by changing the gas composition or increasing the total process pressure [27], [28], [29]. Process pressure and gas composition influence growth and product formation [23], [30], [31]. The hydrostatic pressure at the bottom of industrial fermentation reactors can reach 2 to 3.5 bar with a height of the reactor of about 25 m [32]. This makes the influences of high pressure on the fermentation organism especially important for these applications. The substrate gas composition varies when waste gases or the product gases of other CCS or CCU technologies are used as feedstock for gas fermentation [33]. These limitations, coupled with the inherent nonlinearity and complexity of bioprocess systems, present significant challenges to achieve robust operation. As a result, control strategies are crucial for effectively addressing these issues [34]. In addition to the heterogeneity in gas composition, the limited availability of measurement data during operation represents another

common obstacle. Usually, only delayed, irregularly sampled online, or event-based at-line sensor data is available, for example [25], [35]. Since most advanced control strategies, such as Model Predictive Control (MPC), rely on knowledge of the entire state information, state observer, also known as soft sensors, are an integral component of those control architectures [36], [37], [38]. Soft sensors can assist in reconstructing missing state information. Their performance is highly dependent on the quality of the underlying process model. For this reason and to enable model-supported process design for evaluating the feasibility of fermentation technologies alongside monitoring and controlling the fermentation process, a high-quality model is needed [39]. Many genomic-scale and kinetic models for gas fermentation have been published [40], [41], [42], [43], [44], [45]. However, few models have been tested under continuous cell retention or pressurized conditions, which are beneficial for industrial applications or for the coupling of gas fermentation with the gas streams of other CCS and CCU technologies. Therefore, this study uses a kinetic model by *Medeiros et al.* to model elevated pressure and continuous cell retention conditions as published by *Perret et al.* to enable model-supported process design and optimization [24], [25], [46]. After validating the model's predictive capability, it is applied to investigate the influence of gas residence time (GRT) on substrate gas composition for the production of biomass, ethanol, or acetate.

2. Materials and Methods

2.1 Kinetic Model

2.1.1 Short model overview

In this study, a literature kinetic model published by *Medeiros et al.* was used as a basis and adapted to new process conditions [46]. The model equations can be found in the original publication and in the supporting information, equations S1-S29. The model dynamically approximates a continuous stirred tank reactor with and without cell retention conditions. It consists of differential balance state equations that consider flow balance equations and gas-liquid mass transfer, if necessary. The model further considers the uptake/production rates of CO, H_2, CO_2, EtOH, HAc, and water (H_2O) species in the gas and liquid phases, as well as the biomass concentration in cell dry weight (CDW) in the liquid phase (Equations S1-S5). Gas flow out of the reactor and mass transfer coefficients (kLa) are also approximated with model equations S23-S29. Cell retention is approximated by a purge factor X_p in biomass mass balance. This factor ranges from 0, full cell retention, to 1, full cell purge out of the reactor. Cell growth is described as a function of cell death, which is approximated with a time and activity-independent death rate k_d and growth rate μ. The growth rate is dependent on biomass yield coefficients and H_2 and CO uptake rates (Equations S9), which follow Michaelis-Menten kinetics with substrate and product inhibition (S10). Ethanol inhibition I_E, acetate inhibition I_A, and CO inhibition I_{CO} follow standard non-competitive enzyme inhibition (Equations S11-S14). Hereby, it is assumed that CO only inhibits H_2 uptake. Ethanol inhibition is only implemented into the model with a threshold of 35 g l^{-1} ethanol. For all other substrates and products, the uptake and production rates follow the stoichiometry of the proposed acetate and ethanol production reaction of *C. ljungdahlii* (Equations 1-4) and are combinations of the acetate to ethanol conversion rate $v^R_{EtOH,\,i}$ and the CO or H_2 uptake rates v_i (Equations S15-S22). The model assumes ethanol to be exclusively produced via the AOR route out of acetate and not through the direct ALDH route, and therefore, ethanol production is only possible through acetate conversion and dependent on the acetate concentration. Finally, the model requires 15 kinetic input parameters, which have to be estimated with data, as they incorporate effects not directly described by the model [46].

2.1.2 Model limitations

The mechanistic model does not explicitly represent the effects of all process conditions on fermentation. Instead, these effects are implicitly integrated into the kinetic parameter values. This encompasses the impacts of temperature and pH on microbial growth and product formation, as well

as the influence of culture medium composition on the volumetric mass transfer coefficient (kLa) and growth kinetics. Other process conditions can only directly affect certain parameters. For instance, pressure only affects gas solubility and volume flow, but does not directly affect the biological metabolism kinetics. The model can describe some short-term effects, such as a stirrer failure or a stop in the liquid feed flow rate, but implementation is limited to setting the corresponding parameter to or close to zero for the duration of the effect. Other effects, such as non-ideal mixing in the reactor or time-varying properties like changes in liquid volume, were not incorporated into the model. Process conditions affecting the kinetic model parameters for only short periods of fermentation time cannot be described with the model, because the kinetic parameters were assumed to be time-independent. These effects include the influence of foam formation at high gas flow rates and changes in nutrient composition over long batch fermentation times and at high biomass concentrations.

2.1.3 Model adaptations

The kinetic parameters were re-estimated in this study due to different experimental conditions because they account for effects that were not directly incorporated into the model. Some additional changes were made to the model before these estimations:

1. The ungassed power number N_P used in the original publication for the calculation of power input was approximated with the Newton number N_e following equation 7, wherein Q_G is the gas flow in $m^3\ s^{-1}$, N is the agitation rate in s^{-1}, and d_R and d_i are the reactor and stirrer diameter in m, respectively [46], [47].

$$Ne = 1.5 + \left(0.5 \times \left(\frac{Q_G}{N \times {d_i}^3} \times \left(1 + 38 \times \left(\frac{d_R}{d_i}\right)^{-5}\right)\right)^{0.075} + 1600 \times \left(\frac{Q_G}{N \times {d_i}^3} \times \left(1 + 38 \times \left(\frac{d_R}{d_i}\right)^{-5}\right)\right)^{2.6}\right)^{-1} \quad (7)$$

2. The power input P_V was calculated with equation 8 and the liquid volume of the reactor V_L in m^3 instead of using equation 27 of the original publication [46].

$$P_V = \frac{Ne \times \rho_L \times N^3 \times {d_i}^5}{V_L} \quad (8)$$

3. Ethanol inhibition was implemented without a threshold concentration, even though the ethanol concentration was lower than the threshold concentration proposed for the original model throughout the fermentation experiments used for parametrization and validation. [24], [25], [46]. The original threshold implementation was based on the findings of *Ramio-Pujol et al.* and *Phillips et al.* [35], [48]. *Ramio-Pujol et al.* did not observe a significant ethanol inhibition of *C. ljungdahlii* at concentrations below 15 g l^{-1} ethanol, while *Phillips et al.* observed a sharp decline in cell growth after an ethanol concentration of 35 g l^{-1} was reached [35], [48]. This decline could also be caused by other changes in medium content [35]. To our knowledge, no further investigations were made into ethanol inhibition of *C. ljungdahlii*, but a slight inhibition of the gas uptake rates by ethanol might be possible and was therefore implemented into the model.

4. All 15 kinetic parameters were re-estimated with new experimental datasets, because the different experimental conditions are expected to affect additional parameters, such as inhibition constants or maximum uptake rates. The parameter bounds for these parameters are listed in Table S1 and are directly adopted or based on the bounds published for the original model [46].

The adapted model could not sufficiently predict changes in biomass concentration or changes in the ethanol-to-acetate ratio during the parameter estimation routines. This was predominantly observed at cell retention conditions with GRT lower than 0.26 h (gas flow rates higher than 7 l h^{-1}), and higher CO_2 than CO content in the substrate gas. For this reason, further adaptations were made to the model.

5. A CO_2 dependency was added to the H_2 uptake rate according to standard multi-substrate Michaelis-Menten kinetics, changing equation S9, for H_2, to equation 9. This was done to account for potential effects of CO_2 on H_2 uptake and the growth rate, and limit growth without a carbon source.

$$\nu_{H2} = -\nu_{max,\,H2\,CO2} \times \frac{C_{L,H2}}{C_{L,H2} + K_{H2}} \times \frac{C_{L,CO2}}{C_{L,CO2} + K_{CO2}} \times I_E \times I_A \times I_{CO,H2} \quad (9)$$

6. The acetate to ethanol conversion rate was modified by adding a CO_2 inhibition term (equation 10), to capture the shifts in the ethanol-to-acetate ratio observed in the fermentation experiments used for parametrization under GRT conditions higher than 0.26 h and mild pressure conditions [24], [25]. When *C. ljungdahlii* grows on pure CO or with high CO to CO_2/H_2 ratios in the substrate gas, more ethanol is produced [23], [49]. One possible explanation for this is that *C. ljungdahlii* can synthesize more ATP when grown on CO [49]. *Hermann et al.* also observed higher production of acetate than ethanol when *C. ljungdahlii* was grown on H_2/CO_2 instead of CO in batch cultivations, also citing a lower ATP yield as the main reason for this effect [30]. In this study, it was assumed that the lack of ATP generation with CO_2 as the carbon source can be correlated with the CO_2 concentration in the liquid phase. This was implemented with ethanol production being inhibited by the CO_2 liquid concentration.

$$\nu^R_{EtOH,i} = 0.5 \times \frac{|\nu_i|}{1 + \frac{|\nu_i|}{2 \times \nu^R_{max_{Ac,i}} \times \frac{C_{L,HAc}}{C_{L,HAc} + K^R_{S,AC,i}}}} \times \frac{1}{1 + \frac{C_{L,CO2}}{K_{I\,CO2\,Ac}}} \quad \text{i=CO, } H_2 \quad (10)$$

2.2 Case studies used for the estimation of the kinetic parameters

Product, biomass, and off-gas concentration data from *Perret et al.* 2023, Experiment A and *Perret et al.* 2024, Experiment A was used to estimate model parameters [24], [25]. Hereafter, these experiments are named dataset 1 and dataset 2. The process conditions are provided in Table 1 and Figure S1. The model was only parametrized to time points where every parameter was measured, including gas data. Data from both experiments was used for the parameter estimation routines. The kinetic parameters of models 4 and 5 were estimated with dataset 1 and conditions with pressure ranges from 1 to 2 bar absolute from dataset 2 (80 data points). The purge factor X_P was not specified by *Perret et al.* but was approximated with the ratio of the purged sample volume over time (0.00208 l h^{-1}) to the flow rate [24], [25]. This resulted in an X_P value of 0.0316. The parameter values reported for the original model were used for those not specified for datasets 1 and 2. [24], [25], [46].

Table 1: Short overview of the experimental conditions used for parameterization of the models

Experiment	dataset 1; *Perret et al.* 2023 A [25]	dataset 2; Perret et al. 2024 A [24]
Temperature in °C	37	37
pH	5.85	5.85
Number of different data points	66*6	112(80)*6
Process time in h	1640	1970
Cell retention activation time in h	913	0
Purge factor X_P	0.0316	
Pressure absolute in bar	0	0-4 bar

Gas flow in l h^{-1}	4.8-7.38	5.82-16.5
Liquid flow in l h^{-1}	0-0.066	0-0.066

2.3 Numerical modeling

The original model and the modified models were implemented in MATLAB version: 24.1.0.2603908 (R2024a). The solver ode15s for stiff problems was used for computationally efficient integration of the differential equation system. The kinetic parameters were estimated by minimizing the squared norm of the residuals error. To this end, the global optimization toolbox function *MultiStart* was employed together with the optimization toolbox function *lsqcurvefit*, a nonlinear least squares solver, to find global solutions for the minimization problem. Alongside this, *lsqcurvefit* was used on its own to define local minima. The concentrations of biomass, ethanol, acetate, CO, CO_2, and H_2 used for estimation were weighted by multiplication with a proportional factor to reduce reliance on one component. These constants for the respective concentrations were chosen so that their order of magnitude corresponds to biomass concentration. The proportional factors are listed in Table S2. The absolute tolerance of the ode15s solver was set to 10^{-3} during the parametrization of models 1-4 due to simulation instabilities with lower absolute tolerance. An F-test to discard the null-hypothesis for the model parameters was performed, and 95% confidence intervals of nonlinear regression were estimated for the kinetic parameters. This was done by implementing the procedure detailed by *Medeiros et al.* in MATLAB [46]. Original and re-estimated model parameters and confidence intervals are shown in Table S3 and Table S4, as well as the squared norm of the residuals error in Table 2.

Model validation was followed by steady-state predictions for different substrate gas compositions and GRTs. The models' differential equations were solved using the ode15s solver with the initial conditions of dataset 1 over a time interval of 1000 h to satisfy steady state criteria.

2.4 Model validation with long-term continuous fermentation experiments

The models' performance was compared to two continuous fermentation experiments. The organism, medium composition, experimental setups, and experimental conditions are detailed in the following chapter.

2.4.1 Bacteria, media, and pre-culture

Clostridium ljungdahlii (DSM 13528) was cultivated anaerobically in modified Tanner medium in three pre-cultures and one main culture. A detailed description of the medium composition can be found in *Stoll et al.* [50]. Fructose was added as a carbon source to the pre-cultures to a final concentration of 10 g l^{-1} for pre-culture 1 and 5 g l^{-1} for pre-cultures 2 and 3. Mixtures of artificial synthesis gas were the only carbon source for the main cultivation. The pH of the medium was adjusted to 5.9-6.0 through the addition of KOH pellets. Subsequently, the medium was deoxygenated by sparging with a sterile 20% CO_2 and 80% nitrogen (N_2) gas mixture for 30-60 min. Afterwards, the medium was autoclaved at 121 °C for 25 min, before a sterile 100 g l^{-1} cysteine-HCl solution was added to the medium to a final concentration of 1 vol-% for pre-culture media and 0.3 vol-% for the main culture medium. Pre-cultures were cultivated at 37 °C without stirring in 100 ml serum bottles containing 50 ml medium for 2 days or in the case of pre-culture 3 for 3 days in 500 ml bottles containing 250 ml medium. Pre-culture 1 was inoculated with 10 ml of a starter culture made from a freeze-dried culture stored at -80°C. Pre-cultures 2 and 3 were inoculated with 10 vol-% and 1 vol-% inoculum of the prior pre-culture, respectively. The main cultivation was inoculated with 250 ml of pre-culture 3.

2.4.2 Experimental setup of the fermentation experiments

Experiments were carried out in a heated, 4 l stainless steel continuous stirred tank reactor (CSTR) with continuous gas and liquid flow, a gas mixing station, and an external cell retention circuit. The gas flow rate, gas composition, liquid flow rate, pressure, temperature, and pH are control variables and can be adjusted. The detailed setup is described in *Perret et al.,* and a simplified schematic of the reactor setup

is shown in Figure 1 [24], [25]. A micro annular gear pump (HNP Mikrosysteme, Germany) was used instead of the peristaltic pump described by *Perret et al.* for the cell retention circuit and kept at a flow of 10 l h^{-1} [24], [25].

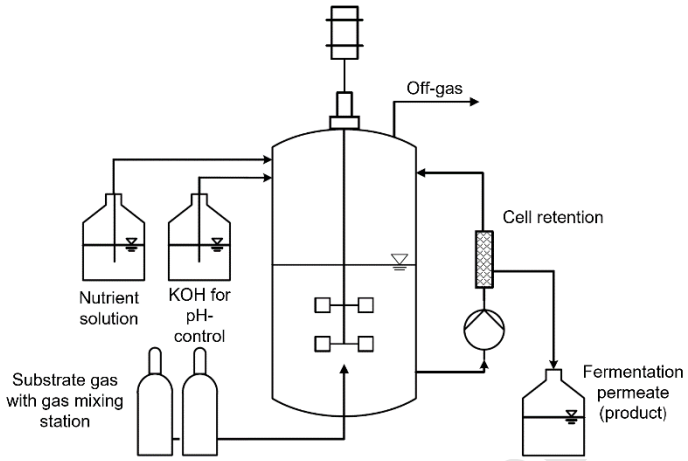

Figure 1: Schematic representation of the fermentation setup; adapted and modified from *Perret et al.* [24]

The reactor, feed pipes, and the cell retention circuit were sterilized prior to inoculation by first filling them with 0.5 % peracetic acid. After this, the reactor was autoclaved by holding the reactor temperature at 120 °C for at least 25 min. This was achieved by blowing hot steam into the reactor at multiple ports. During the experiments, online gas measurements were carried out every 15 min, using a 2-channel gas chromatograph (Inficon Fusion, INFICON, USA) with argon and helium as carrier gases. Off-gas concentrations and flow rates were calculated based on the nitrogen volume fraction in the inlet and off-gas streams and the substrate gas mass flow. Biomass and the product concentration in the reactor broth were monitored daily via manual sampling. The optical density (OD) of the samples was measured with a UV-Vis spectrometer (VWR, Germany) at 600 nm. For this, the samples were diluted with 0.9 vol-% NaCl solution to an OD below 0.4 and measured. The OD of the cell-free samples was determined after centrifugation of the samples for 15 min at 12000 g. The CDW was then estimated by a CDW OD correlation. The ethanol and acetate content of the samples was determined by high-pressure liquid chromatography (HPLC) (Aminex HPX-87-H column, Hitachi, Japan) with an eluent containing 4 mmol l^{-1} sulfuric acid after centrifugation of the undiluted sample.

2.4.3 Experimental conditions of the validation experiments

In the fermentation experiments, the gas composition, gas flow rate, liquid flow rate, pressure, and purge factor were varied over time (see Table S5, Figure 2). All other process conditions were kept constant. The reactor was filled with 2.2 l medium and stirred at 600 rpm. The pH and temperature were held constant at 5.85 and 37 °C, respectively. For experiment A, the previously introduced purge factor used for the model predictions was determined using equation 11 with the OD of the sample taken from the reactor and the OD measured in the permeate at the time of sampling.

$$X_{P,Experiment\ A} = 1 - \frac{OD_{Bioreactor} - OD_{Permeate}}{OD_{Bioreactor}} \quad (11)$$

This resulted in a purge factor of 0.8. Short failures of the liquid feed pump and the stirrer occurred during experiments A and B. The times at which this occurred are shown in Figure 2 and are noted in the affected interval in Table S5.

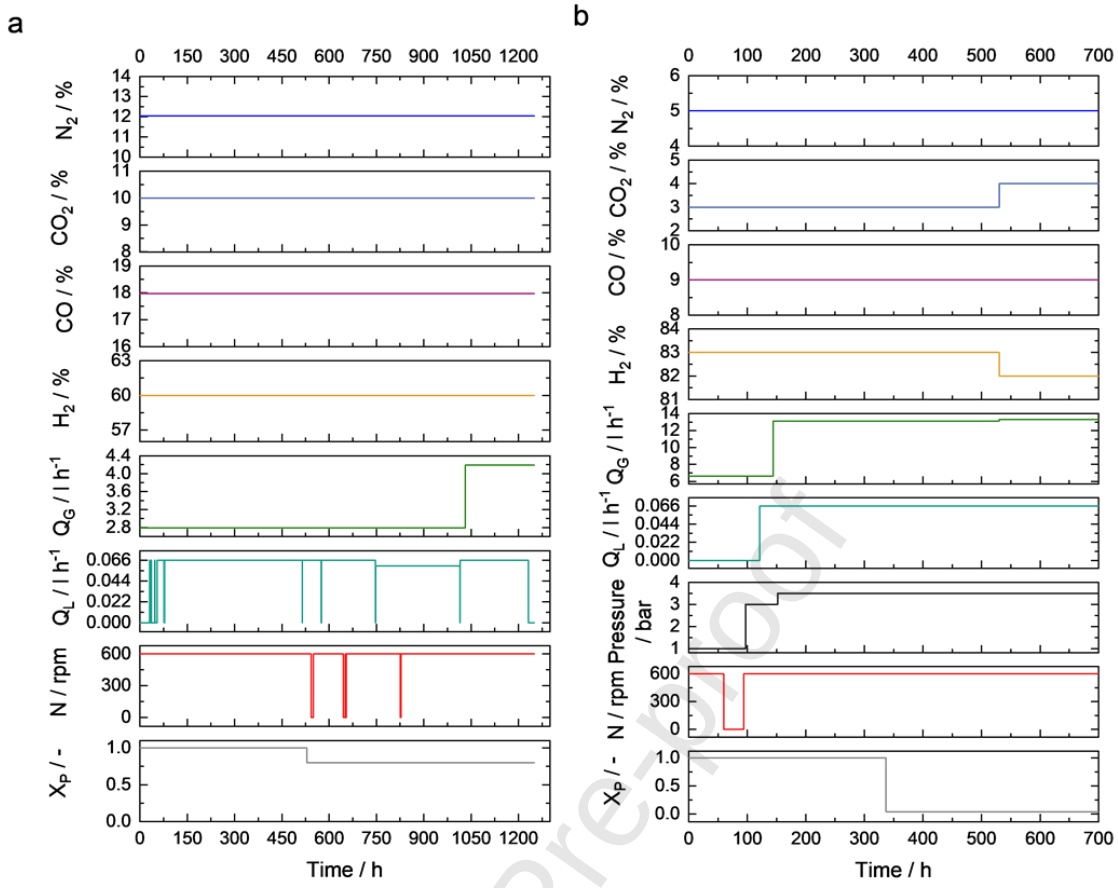

Figure 2: Experimental conditions of the validation runs conducted at 600 rpm, 37°C, and pH of 5.85 for (a) Experiment A, (b) Experiment B; Purge factor Xp, agitation rate N in rpm, reactor pressure in bar, liquid flow rate at 37°C Q_L in l h^{-1}, substrate gas flow rate at 37°C and atmospheric pressure Q_G in l h^{-1}, and substrate gas composition in % over the fermentation time in h

3. Results and discussion

3.1 Parameter estimation and model fit

The changes detailed in Chapter 2.1.3 Model adaptations" and stepwise model iterations are shown in Table 2. The main models discussed in this study are models 3 and 5, representing the models with minor and major applied changes to the base model, respectively. The parameters estimated in this study are significant with respect to the F-test (Table S4) and have mostly low confidence interval errors below 25% (Table S3). Exceptions are the CO uptake affinity constant for CO $K_{S\,CO}$, and the H_2 uptake affinity constant for CO_2 K_{CO2}, with an error greater than 50% in model 5. A possible reason is the small value of $K_{S,\,CO}$, as well as the number of parameters affecting CO and H_2 uptake directly (5-6 parameters). In the case of $K_{S,\,CO}$, the estimation results are close to the set bounds of the parameter. This indicates that the proposed bounds are not optimal. The bounds used in this study are based on those of the original model publication, which were set to align with literature findings at the time. Maximum uptake rates reportedly vary [30]. Therefore, a change in boundaries may improve the accuracy of the model fit, but was not further tested in this study.

Table 2: Adapted and modified models, with short description, model number, the squared norm of the residuals for the model fits, and the squared norm of the residuals for the model fits with less data, absolute, and in % compared to model 1

Parameter	First 7 parameters the same as C1 [46] without $K_{I,ETOH}$	First 7 parameters the same as C1 [46]	Adapted	Adapted less data	Adapted with CO_2 dependency less data
Model Number	1	2	3	4	5
2.1.3 Model adaptations	1-2	1-3	1-4	1-4	1-6
Squared norm of the residuals error all data; only 1-2 bar	633; 452	548; 452	387; 287	479; 253	454; 173
Squared norm of the residuals error all data; only 1-2 bar in %	100; 100	86; 100	61; 63	76 ;56	72; 38
Notes				only pressure condition 1-2 bar for fit	only pressure condition 1-2 bar for fit

Model 3 (Figure 3, green line) can approximate the general trends in dataset 1 for biomass, ethanol, and acetate concentration as well as CO, CO_2, and H_2 concentration in the reactor off-gas with sufficient accuracy until 1200 h. After this point, a drop in both biomass and ethanol concentration is observed in the experiment, which the model cannot predict (Figure 3.A-F green line and black squares). The higher CO and CO_2 content present in the substrate gas at this time may be a reason for this drop in biomass and ethanol concentration. CO inhibition is already implemented in the original model, which is why other effects most likely cause the drop in biomass and ethanol concentration. Most likely, CO_2 also has inhibitory effects that are not yet described in the model. This can be observed at approximately 600-700 h in dataset 2 under moderate pressure conditions. A decline in biomass and ethanol concentration and an increase in acetate concentration followed the increase of CO_2 substrate gas concentration, whereby the gas flow rate and the other gas components were slightly changed (Figure 3 g-j; Figure S1 b). A loss in cell activity as a result of non-ideal reactor conditions caused by foam formation resulting from the high gas flow rate greater than 7 l h^{-1} (GRT 0.26 h), documented at this time, is also possible, as foam formation affects various fermentation parameters [51]. The model represents the general gas data trend of dataset 2, especially for CO, while overpredicting the amount of CO_2 and underpredicting the amount of H_2 in the reactor off-gas, but can still capture the dynamic responses and changes of the gas data used for the estimation (Figure 3.J-L). The model is unable to portray the changes in the ethanol-to-acetate ratio under pressure conditions with simultaneous high gas flow rates greater than 9 l h^{-1} (GRT smaller than 0.2 h) and follows a trend line for biomass, ethanol, and acetate concentration (Figure 3.G-I). The model only responds to the general increase in gas flow rate and pressure, while it cannot depict the changes in the ethanol-to-acetate ratio and biomass concentration resulting from variation in the substrate gas composition. This indicates that the acetate to ethanol conversion/ethanol production of the model is not accurate for high gas flow, cell retention, and pressurized conditions. To address the inability of model 3 to accurately describe the off-gas concentration and the ethanol-to-acetate ratio at high gas flow rates, further model adaptations were tested. To mitigate the effect of unknown influences of high pressure on the fermentation of *C. ljungdahlii,* model 4 was only fitted to pressure conditions smaller than 3 bar. This resulted in a decrease in error (Table 2), but model 4 is still unable to accurately capture the changes in biomass, ethanol, and acetate production at moderate pressure conditions and gas flow rates greater than 7 l h^{-1}. A likely cause is an inhibitory effect of CO_2 on the growth rate and the acetate to ethanol conversion. This effect was implemented in model 5, as detailed above.

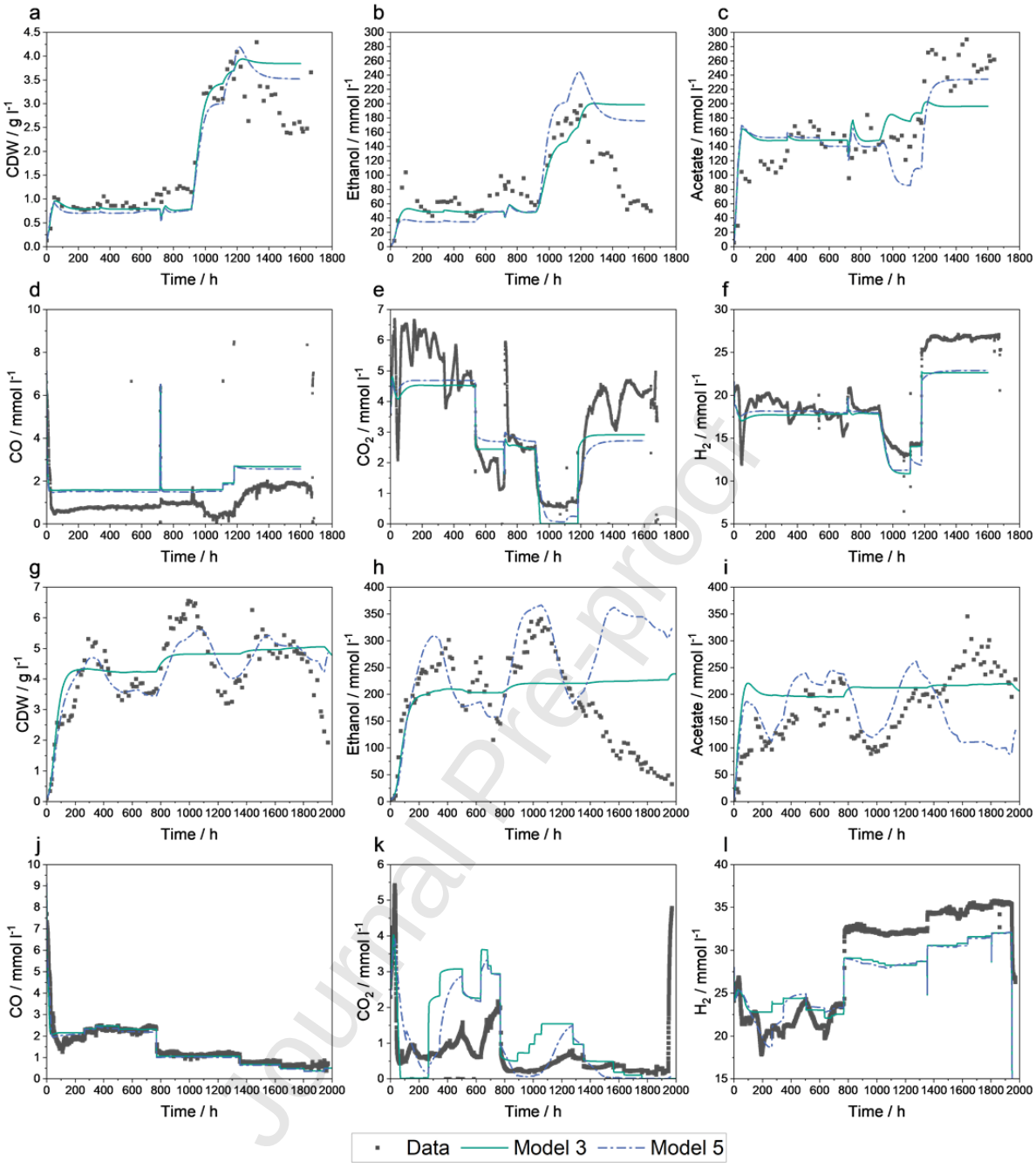

Figure 3: Model predictions and comparison to biomass concentration in g l^{-1}, ethanol and acetate concentration in the liquid phase in mmol l^{-1} and CO, CO_2 and H_2 concentration in the off-gas in mmol l^{-1} for dataset 1 [25] (a-f) and dataset 2 [24] (g-l) over the fermentation time in h; Green line re-estimated model with ethanol inhibition (Model 3), blue line modified model with CO_2 dependency and inhibition (Model 5)

Model 5 was fitted to datasets 1 and 2 under moderate pressure conditions (1-2 bar). The parameter estimation results for model 5 are presented in Table 2, and the model fit is illustrated in Figure 3 (blue line). This modification results in a 30% lower squared norm of the residuals error compared to the model fit of model 4, which was estimated under the same conditions. Compared to models 3 and 4, it provides a better approximation of the dataset trends (Figure 3). Model 5 depicts the biomass and acetate concentration trend similar to model 3 and exhibits a slightly worse ethanol concentration depiction in the first 600 h of dataset 1 than model 3 until cell retention is activated. Afterwards, all

product concentrations are more accurately portrayed by model 5. This model can even portray the first decrease in biomass and ethanol concentration observable in dataset 1 after 1200 h as a result of the increased CO_2 concentration in the substrate gas, but fails to predict the second decrease observed without a change to the prior process conditions at 1400 h. This indicates that the second drop is likely caused by a loss in activity of the cells, changes in media nutrients, or other unimplemented changes of the reactor setup, such as foam formation, or time-dependent changes to the model parameters, as detailed above, and cannot be predicted with the current model, as discussed in 2.1.2 Model limitations.

Model 5 also follows the biomass, ethanol, and acetate concentration of dataset 2 under pressure conditions smaller than 3 bar more accurately than model 3 (Figure 3.G-L). As mentioned earlier, model 3 only responds to some dynamic changes of dataset 2, primarily the increases in gas flow rate and pressure. In comparison, model 5 can portray changes in biomass, acetate, and ethanol concentration resulting from variations in the substrate gas composition in dataset 2. This shows that the changes in product ratio and biomass concentration observed in this experiment are likely caused by the effects of changing the substrate gas composition, especially the CO_2 content, and can be approximated with the model modifications proposed. The biomass and off-gas concentration trends of model 5 follow the data trends under pressurized conditions not used for fitting (Figure 3.G-L after 1400 h). Despite this, the model cannot predict the trend of ethanol and acetate production under these conditions. Ethanol concentration is overestimated, and acetate concentration is underestimated. For most of the fermentation time, the trend of ethanol concentration follows the trend for the biomass concentration. Growth and ethanol production in *C. ljungdahlii* are reported to be closely correlated, which explains this behavior [52]. At pressures above 2 bar, this behavior switches from ethanol to acetate. Therefore, the low GRT, high-pressure conditions affect the metabolism of the bacteria in a way not implemented into the model. The assumption of ethanol being only produced via the AOR route in the original model is based on the findings of *Richter et al.*, who reported ethanol to be exclusively produced with this route in a CSTR and bubble column reactor with CO as the main gas component [53]. Nevertheless, the acetate conversion and ethanol production can change under high-pressure conditions. For example, a production of ethanol via the ALDH route might occur. This was tested by implementing a direct production of ethanol out of the substrate gas with standard Michaelis-Menten kinetics (data not shown). No significant effect of this change on the model performance was observed, which is why this approach was not further investigated. Another theory for the observed shift in the ethanol-to-acetate ratio is a possible inhibitory effect of H_2 in the liquid phase on the production of ethanol [24]. This effect is not described for *C. ljungdahlii* under mild pressure conditions. *Demler et al.* observed in batch experiments with *Acetobacterium woodii* that higher partial pressures of H_2 yield more acetate [54]. This could be the case for *C. ljungdahlii* under high-pressure conditions due to the increased solubility of H_2 and has to be investigated in future research.

A pressure-dependency of the acetate to ethanol conversion rates, and an addition of inhibition by H_2-concentration in the liquid phase were tested for this purpose (models 6 and 7; change of equation 10 to equation S30 or S31, respectively). Both changes approximated the acetate and ethanol concentration under high-pressure conditions with smaller errors than prior model iterations, reducing the overall squared norm of the residuals error by about 40% when compared to model 3. However, the representation of biomass under high-pressure conditions and the behavior of the acetate concentration over the fermentation time of dataset 2 (Figure S2) were less accurate than model 5s simulations. These results suggest that further model adjustments are necessary to accurately predict high-pressure cultivations .

Other untested hypotheses that might cause the shift in the ethanol-to-acetate ratio include a loss in microbial activity or a change in death rate. Pressure influences cell activity, genome expression, product spectrum, and death rate in other microorganisms [55], [56], so this is likely for *C. ljungdahlii*. For instance, *Sivalingam et al.* observed an increase in acetate and volatile fatty acid production in batch experiments with mixed acetogen cultures when H_2 pressure was increased up to 15 bar [57]. *Oswald et al*. observed that *C. ljungdahlii* produces formic acid under high-pressure conditions above 7 bar [31]. Formic acid is an intermediate product in the WLP, and its production was also observed by *Perret et al.* in small concentrations up to 0.1 g l^{-1}[24]. Due to this small amount, formic acid production was not implemented into the model, as a significant influence is unlikely. Various microorganisms react differently to environmental stress conditions and adapt their metabolism accordingly [58]. In the study used for parametrization, *C. ljungdahlii* was cultivated under cell retention, pressure conditions for a long time. Hence, there is a high chance that the microorganisms adapted to the pressure conditions, which are not suitable for maximum metabolic activity, by reducing ATP usage. This resulted in lower ethanol production and yield, because *C. ljungdahlii* shifted its metabolism to maintain biomass and save ATP by reducing ethanol production. Ethanol production in *C. ljungdahlii* is proposed to be an overflow mechanism of high reduction equivalents and acetic acid concentrations [53]. While high acetic acid concentrations were produced under high-pressure conditions, the cells were exposed to more stress caused by the high pressure, with a possible manifestation in a higher death rate, in reduced substrate yields, or in lower reduction equivalent concentration and, consequently, lower ethanol production and higher acetic acid production. This indicates a time dependency of the kinetic parameters, which cannot be described with the current model setup. One solution is a segmented model approach over the fermentation time, meaning re-estimating important parameters, such as the death rate or parameters linked to ethanol production, under high-pressure conditions, instead of using a single model with the same estimated kinetic parameters or rate equations for all fermentation conditions. However, a better general understanding of pressure effects on growth and product formation in *C. ljungdahlii* is necessary for further model modifications.

The predictions of model 5 for the off-gas concentrations are similar to those of model 3, despite the changes to the H_2 uptake rate in model 5. The main difference is the H_2 concentration in the off-gas during the first 300 h of dataset 2, where model 5 portrays a decrease in H_2 off-gas concentration, observed in the study, but not predicted by model 3. Another difference is the CO_2 off-gas concentration in the same dataset, which is approximated more accurately by model 5. These changes resulted from the changes to the acetate to ethanol conversion rate and the added dependencies of CO_2 concentration on H_2 uptake. All models approximate changes caused by the stirrer failure occurring at approximately 700 h cultivation in dataset 1, but predict a shorter influence on the acetate concentration than observed. In the model, a stirrer failure is implemented by setting the agitation rate to 0 for a given duration with no additional changes. The CSTR reactor is still assumed to be ideally mixed. In reality, various changes could influence the microorganisms [59], [60]. Such changes may involve cell sedimentation, and several gradients of e.g., temperature, pH, and nutrients, ultimately evoking metabolic adaptation, loss of activity, cell starvation, or death.

3.2 Validation of the model prediction capabilities

Two experiments were conducted in the same reactor setup used by *Perret et al.* and compared with predictions of model 3 and 5 made for these conditions (see Table S5 and Figure 2 for the detailed conditions and Figure 4 for the comparison of the model prediction and experimental data) [24], [25]. All models can predict the general trends in both fermentation experiments. The predicted biomass concentration follows experiments A and B closely until activation of cell retention. In experiment A, this discrepancy might be caused by a stirrer failure shortly after cell retention was enabled. This could also explain the overestimation of biomass concentration in the first hours of experiment B (Figure 4).

In experiment A, model 3 provides the best approximation of biomass over the whole fermentation time, while in experiment B, model 3 predicts nearly double the amount of biomass concentration observed under pressurized, cell retention conditions. This is likely caused by the low gas rate and high purge factor conditions in experiment A, which are well-described with the unmodified model, while the high pressure and low purge factor conditions in experiment B need further model modifications to be accurately described. Although model 5 portrays the biomass concentration in experiment B more accurately, it cannot predict the decline in biomass concentration observed after 500 h. This is caused by the high-pressure conditions of 3.5 bar absolute in this experiment, which are not adequately portrayed in the models.

Model 3 predicts the trend of ethanol concentration more accurately than model 5, which tends to underestimate ethanol production. In experiment B, this changes after 500 h at high pressures and CO_2 concentrations, where model 5 matches the observed ethanol concentration closer than model 3, the latter predicting a further increase in ethanol concentration, which is not observed during this experiment. This indicates that the changes to the acetate conversion positively influence the predictive capability of the models under these conditions. In experiment A, predictions for acetate concentrations were similar for all models, with all of them overpredicting acetate concentration. An exception to this is an increase in acetate concentration after 1100 h observed in experiment A as a result of the higher gas flow rate, which is only predicted in model 5.

All models predict off-gas concentrations for H_2, CO, and CO_2 similarly. For experiment A, the CO off-gas concentration is overpredicted, while for experiment B, under pressurized conditions, it is underestimated. A similar trend is observed for the H_2 off-gas concentration. CO_2 off-gas concentration is overestimated in both experiments, with a closer portrayal by model 3. The models approximate simulated stirrer failures, but predict a shorter influence on biomass and product concentration than observed in the experiments, mirroring the model response to the stirrer failure in dataset 1 (Figure 3). Furthermore, the models do not predict the decline in biomass concentration observed in experiment A under batch conditions at the end of the experiment. Nutrient limitations during this phase are a possible cause, as no new fresh medium was fed into the reactor. The effect of media components is not represented within the models. Likewise, all models overpredict the amount of biomass and acetate produced during the initial batch phase of experiment A, caused by a possible prolonged adaptation of the microorganisms to the new conditions, resulting in less growth.

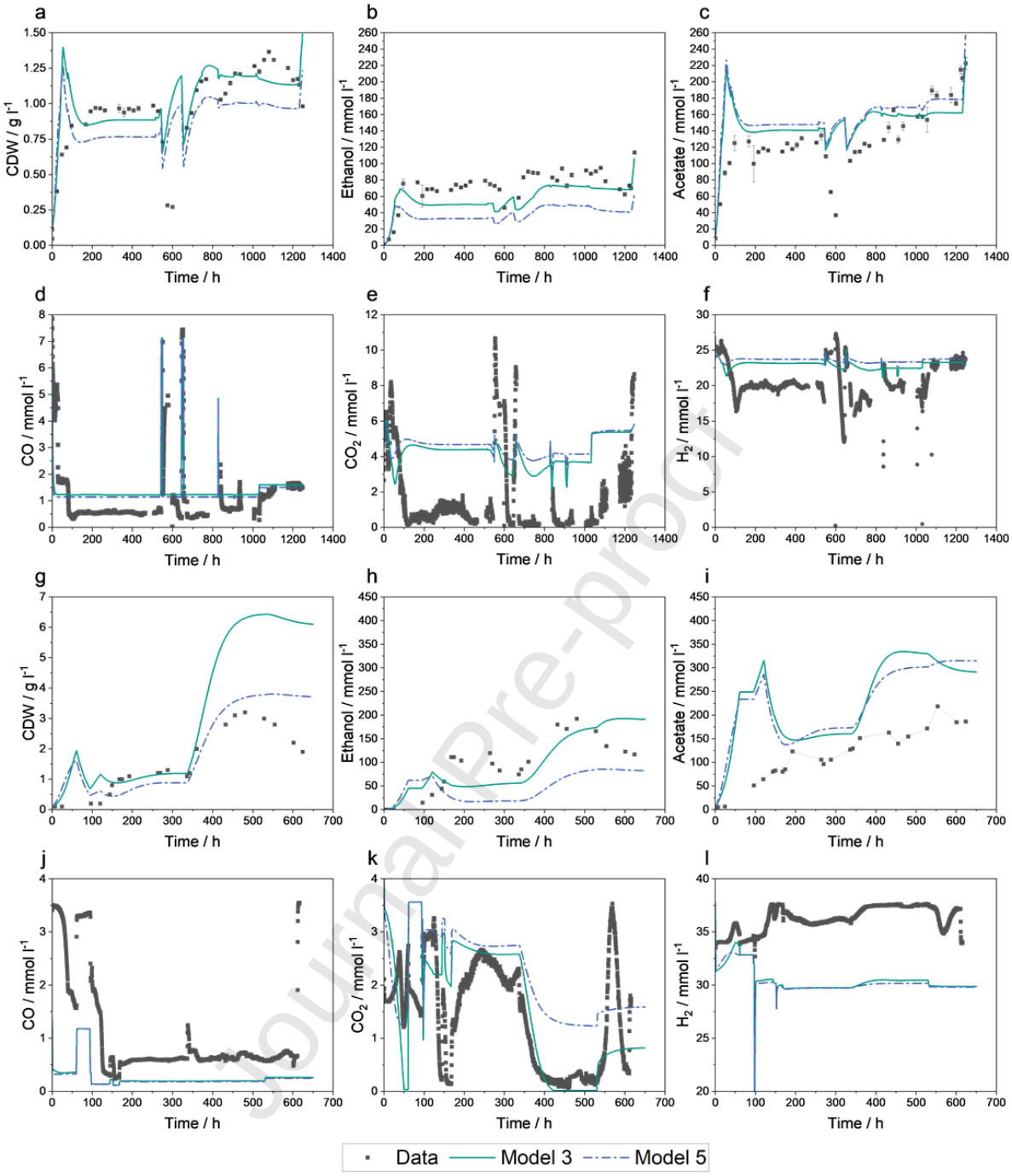

Figure 4: Model predictions and comparison to biomass concentration in g l^{-1}, ethanol, and acetate concentration in mmol l^{-1} and CO, CO_2, and H_2 off-gas concentration in mmol l^{-1} for the validation experiments A (a-f)and B (g-l) over the fermentation time in h; Green line re-estimated model with ethanol inhibition; Blue line modified model with CO_2 dependency and inhibition

In this study, the variation in gas composition in the data used for parametrization and validation was rather small. Experiments were only carried out with H_2 contents in the substrate gas ranging from 60-80% while CO and CO_2 content never exceeded 20%. Therefore, validation of the model with CO, CO_2, and H_2 ratios in the substrate gas outside of these ranges is necessary and will be the focus of future studies. Although model 5 portrays most of the dynamic profiles of the experiments used to estimate and validate the model parameters, it is unable to make accurate predictions under high-pressure conditions. Currently, industrial gas fermentation reactors operate at hydrostatic pressure ranges from

1 to 3.5 bar inside the reactor, which fall within the scope of the modified model [32]. However, this could change in the future, as a higher demand for gas fermentation could necessitate larger reactors. One of the largest airlift reactors was operated with a pressure range of 3 to 6 bar, demonstrating the need for models capable of predicting high-pressure conditions [61]. In order to optimize the model predictions under high-pressure cell retention conditions and to improve the model's predictive capabilities in general, it is necessary to better understand how pressure and cell retention affect the metabolism, viability, and activity of *C. ljungdahlii*. Additionally, further optimization of the model parameterization and kinetics is necessary to incorporate effects found through future experimental research. This requires additional parameterization routines and variation of parameter boundaries, as well as further validation runs to ensure the model's predictive accuracy.

3.3 Predicting the influence of GRT on optimal substrate gas composition for product formation

To test the model's capability as a tool for future process optimizations, predictions were made with the model to determine the influence of GRT on the needed substrate gas composition for high product yield. Model 5 was used to predict the influence of gas composition and GRT on the optimal substrate gas composition for ethanol, acetate, or biomass production in the aforementioned fermentation setup, due to its high accuracy in predicting the dynamic profiles of experiments A and B, as well as datasets 1 and 2, under moderate pressure conditions. These compositions were predicted under the assumption of full cell retention, a continuous liquid flow rate of 0.066 l h^{-1}, no N_2 in the substrate gas, pH of 5.85, temperature of 37 °C, pressure of 1 bar, and agitation rate of 600 rpm. The substrate gas composition with the highest concentration of biomass, ethanol, or acetate at the corresponding GRT is shown in Figure 5.

Model 5 predicts the optimal ratio of H_2, CO, and CO_2 in the substrate gas to change from high CO content conditions of 50% towards lower CO concentrations of 22% with lower GRT for ethanol and biomass production. More CO than CO_2 is estimated to be optimal for ethanol and biomass production, with the optimal ratio being composed of only CO and H_2. The model predicts that these optimal gas compositions for maximum biomass and ethanol concentration follow each other closely. Both are produced when substrate gas consists of 60 to 80% H_2 and 40 to 20% CO, depending on the GRT (Figure 5). An explanation for this is the close correlation between growth and ethanol production in *C. ljungdahlii* [52]. Acetate is mainly produced with a H_2 concentration of 50% and high CO_2 contents in the substrate gas. The latter rises from 10 to 30% with lower GRT, while CO concentration declines simultaneously from 40 to 20% (Figure 5). In general, high CO concentrations are favorable for product formation at high GRT, while high H_2 concentrations are favorable at low GRT. In contrast, the original unmodified model projects high CO concentrations higher than 50% to be advantageous for ethanol production even under low GRT conditions and in batch conditions with a GRT of 0.42 h [46], [62]. These differences are caused by the variation in pH at which the kinetic parameters were estimated, as pH influences the substrate uptake and usage [24]. Model 5 predicts ethanol concentration to rise more than tenfold, from 36 to 456 mmol l^{-1} by lowering the GRT from 3.6 to 0.09 h and a simultaneous increase in H_2 concentration in the substrate gas (Figure 5). These predictions also indicate that acetate concentration rises from 80 to 354 mmol l^{-1} by lowering the GRT and changing the main carbon source of the substrate gas from CO to CO_2 (Figure *5*). These predictions demonstrate that the substrate gas composition and flow rate influence the desired fermentation product and its concentration. This shows that control of the fermentation is possible by varying these conditions, and is essential for optimizing the fermentation process or to integrate the fermentation process with other CCS and CCU technologies.

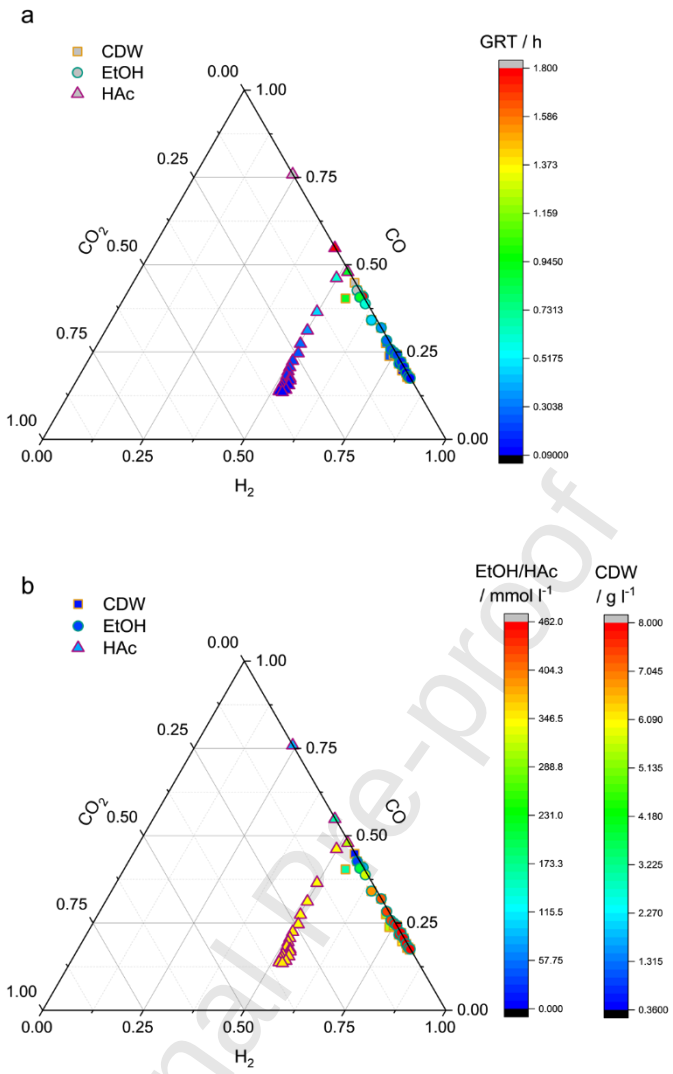

Figure 5: Prediction of model 5 for the optimal substrate gas composition for maximum production of CDW (orange squares), ethanol (green circles) and acetate (purple triangles) for different GRTs from 3.6-0.09 h (gas flow rates from 0.5-20 l $^{-1}$) in the steady state after 1000 h of cultivation; (a) GRT indicated by color in h;(b) Predicted CDW, ethanol and acetate concentration indicated by color in g l^{-1} and mmol l^{-1} respectively; 4 l reactor, 2.2 l liquid volume, full cell retention X_P 0.0316, liquid-flow rate 0.066 l h^{-1}, no inert gas component (N_2) in substrate gas, pH of 5.85, temperature of 37 °C, pressure of 1 bar and agitation rate of 600 rpm; Initial conditions of dataset 1

3.4 Impact of the study

The extended models discussed in this study are based on a model from literature with the aim of optimizing applicability for high hydrogen substrate gas with a mixed carbon source, cell retention, and elevated pressure conditions. The addition of a CO_2 dependency on the H_2 uptake rate and a CO_2 inhibition of the acetate to ethanol conversion rates enabled a more accurate approximation in model 5 when compared to model 3, which emphasizes the significant impact of CO_2 on the metabolism and product formation of *C. ljungdahlii*.

The role of CO_2 is also reflected in the predictions of model 5. Switching the main carbon source from CO to a mixture of CO and CO_2 shifts the main product of the fermentation from ethanol to acetate. This can be beneficial for future gas fermentation applications, as possible substrate gas sources can be selected based on availability and desired product. Therefore, the model can be used to *a priori*

screen the effects of different gas compositions on the fermentation and to determine the feasibility of alternative synthesis gas sources.

Furthermore, this study highlights novel research needs. A detailed understanding of the effects of CO_2 on the product formation and metabolism of *C. ljungdahlii* is required and should be investigated in more depth in future research. Additionally, the model shows that the effect of high pressure on gas fermentation is not sufficiently understood beyond enhancing gas solubility. Discrepancies between the current model predictions and the data used for parameter estimation and validation suggest possible changes in the metabolic activity of *C. ljungdahlii* at high pressure. Hence, future research should also investigate the possibility of inhibition of ethanol production by components that are not typically limiting under non-pressurized conditions, such as H_2. The metabolism of *C. ljungdahlii* at high-pressure conditions and the effect of elevated pressure on ethanol production, such as possible ethanol production via the ALDH route, should also be investigated to enable implementation into the model for improved accuracy in describing high-pressure conditions.

Nonetheless, advancements to the model made in this work allow for conditions with high hydrogen substrate gas, cell retention, and moderate pressures to be described accurately. This enables an expanded application of the model as an optimization and prediction tool under such conditions and can be a step toward using the model for process control.

4. Conclusion

In this study, the literature model proposed by *Medeiros et al.* was adapted to a different reactor setup with different process conditions [24], [25], [46]. Minor modifications to the H_2 uptake rate and the acetate to ethanol conversion rates enabled moderate pressure and high H_2, low CO substrate gas content conditions to be described accurately. The modified models sufficiently predicted the dynamic off-gas and product concentration trends observed in two experiments conducted within the same reactor setup, without having to re-estimate the model's kinetic parameters. Predictions made with the model show promising results for using the kinetic model as a prediction and optimization tool.

Data availability statement

All the data are openly available on Repo4Cat (https://repository.nfdi4cat.org/) via the link: https://hdl.handle.net/21.11165/4cat/XXXX-XXXX.

CRediT authorship contribution statement

C.E. Conceptualization; Formal analysis; Investigation; Methodology; Validation; Visualization; Writing – original draft

L.R. Methodology; Writing – original draft

S.M. Investigation; Methodology; Writing – review & editing

T.M. Funding acquisition; Project administration; Writing – review & editing

A.K. Funding acquisition; Writing – review & editing

M.W. Project administration, Writing – review & editing

J.S. Conceptualization; Funding acquisition; Project administration; Resources; Writing – review & editing

Acknowledgment

The authors thank Elena Hauer and Elias Richter for their support of the experiments, Karl Weiss and Dennis Heidenblut for their technical support, and Veronika Holderied for conducting the HPLC

analysis. The authors acknowledge funding of this work by the Deutsche Forschungsgemeinschaft (DFG, German Research Foundation) NSERC-DFG SUSTAIN SA 2666/2-1. The Helmholtz Association is acknowledged for the funding of S.M. via the research program “Materials Systems Engineering”, topic “Adaptive and Bioinstructive Materials Systems” and the KIT via KIT-Strategy Funding.

Nomenclature

Symbol	Description	Unit
$C_{L, CO2}$	Liquid concentration of carbon dioxide	mmol l^{-1}
$C_{L, H2}$	Liquid concentration of hydrogen	mmol l^{-1}
$C_{L, HAc}$	Liquid concentration of acetate	mmol l^{-1}
$C_{L, i}$	Liquid concentration of component i	mmol l^{-1}
d_i	Stirrer diameter	m
d_R	Reactor diameter	m
I_A	Inhibition acetate	
$I_{CO, H2}$	Inhibition of hydrogen uptake by CO	
$I_{CO, i}$	Inhibition of the uptake of component i by CO	
I_E	Inhibition ethanol	
K_{CO2}	Affinity constant for CO_2	mmol l^{-1}
k_d	Death constant	h^{-1}
K_{H2}	Affinity constant of H_2	mmol l^{-1}
$K_{I\ CO2\ AC}$	Inhibition constant of CO_2 in the acetate to ethanol conversion	mmol l^{-1}
$K^R_{S, AC, i}$	Affinity constant for acetate in the acetate to ethanol conversion	mmol l^{-1}
$K_{S, i}$	Affinity constant for component i	mmol l^{-1}
N	Agitation rate	s^{-1}
Ne	Newton number	
$OD_{Bioreactor}$	Optical density of the sample	
$OD_{Permeate}$	Optical density of the permeate	
p_R	Reactor pressure	bar
P_V	Power input	W
Q_G	Gas volume flow rate	$m^3\ s^{-1}$
Q_L	Liquid volume flow rate	$m^3\ s^{-1}$
X_p	Purge factor	-
$X_{P,\ Experiment\ A}$	Experimentally investigated purge factor	

Symbol	Description	Unit
v_{H2}	Specific uptake rate of H_2	mmol g^{-1} h^{-1}
v_i	Specific uptake rate of component i	mmol g^{-1} h^{-1}
$v_{max, H2, CO2}$	Maximum specific CO2-dependent uptake rate of H_2	mmol g^{-1} h^{-1}
$v_{max, i}$	Maximum specific uptake rate of component i	mmol g^{-1} h^{-1}
$v_{max}{}^{R}{}_{Ac, i}$	Maximum specific reaction rate of acetate uptake dependent on component i	mmol g^{-1} h^{-1}
$v^{R}{}_{EtOH, i}$	Specific reaction rate of the acetate to ethanol conversion with simultaneous use of component i	mmol g^{-1} h^{-1}
μ	Growth rate	h^{-1}

Abbreviations	
ADH	Alcohol dehydrogenase
ALDH	Aldehyde dehydrogenase
AOR	Aldehyde ferredoxin oxidoreductase
CCS	Carbon capture and storage
CCU	Carbon capture and utilization
CDW	Cell dry weight
CO	Carbon monoxide
CO_2	Carbon dioxide
CSTR	Continuous stirred tank reactor
EtOH	Ethanol
GRT	Gas residence time
H_2	Hydrogen
H_2O	Water
HAc	Acetic acid/acetate
MPC	Model Predictive Control
N_2	Nitrogen
OD	Optical density
WLP	Wood-Ljungdahl-Pathway

References

[1] United Nations Environment Programme, “Emissions Gap Report 2024: No more hot air … please! With a massive gap between rhetoric and reality, countries draft new climate commitments,” 2024, doi: https://doi.org/10.59117/20.500.11822/46404.

[2] E. Hanson, C. Nwakile, and V. O. Hammed, “Carbon capture, utilization, and storage (CCUS) technologies: Evaluating the effectiveness of advanced CCUS solutions for reducing CO2 emissions,” *Results in Surfaces and Interfaces*, vol. 18, p. 100381, Jan. 2025, doi: 10.1016/j.rsurfi.2024.100381.

[3] A. I. Osman, M. Hefny, M. I. A. Abdel Maksoud, A. M. Elgarahy, and D. W. Rooney, “Recent advances in carbon capture storage and utilisation technologies: a review,” *Environ Chem Lett*, vol. 19, no. 2, pp. 797–849, Apr. 2021, doi: 10.1007/s10311-020-01133-3.

[4] L. Perret, B. Lacerda de Oliveira Campos, K. Herrera Delgado, T. A. Zevaco, A. Neumann, and J. Sauer, “CO x Fixation to Elementary Building Blocks: Anaerobic Syngas Fermentation vs. Chemical Catalysis,” *Chemie Ingenieur Technik*, vol. 94, no. 11, pp. 1667–1687, Jan. 2022, doi: 10.1002/cite.202200153.
[5] I. K. Stoll, N. Boukis, and J. Sauer, “Syngas Fermentation to Alcohols: Reactor Technology and Application Perspective,” *Chemie Ingenieur Technik*, vol. 92, no. 1–2, pp. 125–136, Jan. 2020, doi: 10.1002/cite.201900118.
[6] P. Dürre and B. J. Eikmanns, “C1-carbon sources for chemical and fuel production by microbial gas fermentation,” *Curr Opin Biotechnol*, vol. 35, pp. 63–72, Jan. 2015, doi: 10.1016/j.copbio.2015.03.008.
[7] F. Liew, M. E. Martin, R. C. Tappel, B. D. Heijstra, C. Mihalcea, and M. Köpke, “Gas Fermentation—A Flexible Platform for Commercial Scale Production of Low-Carbon-Fuels and Chemicals from Waste and Renewable Feedstocks,” *Front. Microbiol.*, vol. 7, May 2016, doi: 10.3389/fmicb.2016.00694.
[8] J. Phillips, R. Huhnke, and H. Atiyeh, “Syngas Fermentation: A Microbial Conversion Process of Gaseous Substrates to Various Products,” *Fermentation*, vol. 3, no. 2, p. 28, Jan. 2017, doi: 10.3390/fermentation3020028.
[9] X. Sun, H. K. Atiyeh, R. L. Huhnke, and R. S. Tanner, “Syngas fermentation process development for production of biofuels and chemicals: A review,” *Bioresource Technology Reports*, vol. 7, no. 4, p. 100279, Jan. 2019, doi: 10.1016/j.biteb.2019.100279.
[10] S. W. Ragsdale and E. Pierce, “Acetogenesis and the Wood–Ljungdahl pathway of CO2 fixation,” *Biochimica et Biophysica Acta (BBA) - Proteins and Proteomics*, vol. 1784, no. 12, pp. 1873–1898, Dec. 2008, doi: 10.1016/j.bbapap.2008.08.012.
[11] M. Köpke, C. Mihalcea, J. C. Bromley, and S. D. Simpson, “Fermentative production of ethanol from carbon monoxide,” *Current Opinion in Biotechnology*, vol. 22, no. 3, pp. 320–325, June 2011, doi: 10.1016/j.copbio.2011.01.005.
[12] N. Fackler *et al.*, “Stepping on the Gas to a Circular Economy: Accelerating Development of Carbon-Negative Chemical Production from Gas Fermentation,” *Annu. Rev. Chem. Biomol. Eng.*, vol. 12, no. 1, pp. 439–470, June 2021, doi: 10.1146/annurev-chembioeng-120120-021122.
[13] A. M. Henstra, J. Sipma, A. Rinzema, and A. J. Stams, “Microbiology of synthesis gas fermentation for biofuel production,” *Current Opinion in Biotechnology*, vol. 18, no. 3, pp. 200–206, June 2007, doi: 10.1016/j.copbio.2007.03.008.
[14] Y. Cui, K.-L. Yang, and K. Zhou, “Using Co-Culture to Functionalize Clostridium Fermentation,” *Trends in Biotechnology*, vol. 39, no. 9, pp. 914–926, Sept. 2021, doi: 10.1016/j.tibtech.2020.11.016.
[15] N. Dhakal and B. Acharya, “Syngas Fermentation for the Production of Bio-Based Polymers: A Review,” *Polymers*, vol. 13, no. 22, p. 3917, Nov. 2021, doi: 10.3390/polym13223917.
[16] F. Oswald *et al.*, “Sequential Mixed Cultures: From Syngas to Malic Acid,” *Front. Microbiol.*, vol. 7, June 2016, doi: 10.3389/fmicb.2016.00891.
[17] X. Zheng, S. Wang, X. Huang, H. Deng, T. Ai, and Y. Jiang, “Tandem direct carbonate electrolysis with syngas fermentation for multicarbon chemicals production,” *International Journal of Hydrogen Energy*, vol. 105, pp. 1040–1046, Mar. 2025, doi: 10.1016/j.ijhydene.2025.01.428.
[18] A. Rückel, A. Oppelt, P. Leuter, P. Johne, S. Fendt, and D. Weuster-Botz, “Conversion of Syngas from Entrained Flow Gasification of Biogenic Residues with Clostridium carboxidivorans and Clostridium autoethanogenum,” *Fermentation*, vol. 8, no. 9, p. 465, Sept. 2022, doi: 10.3390/fermentation8090465.
[19] R. S. Tanner, L. M. Miller, and D. Yang, “Clostridium ljungdahlii sp. nov., an acetogenic species in clostridial rRNA homology group I,” *Int J Syst Bacteriol*, vol. 43, no. 2, pp. 232–6, Jan. 1993, doi: 10.1099/00207713-43-2-232.
[20] J. L. Cotter, M. S. Chinn, and A. M. Grunden, “Influence of process parameters on growth of Clostridium ljungdahlii and Clostridium autoethanogenum on synthesis gas,” *Enzyme and*

Microbial Technology, vol. 44, no. 5, pp. 281–288, May 2009, doi: 10.1016/j.enzmictec.2008.11.002.

[21] A. Infantes, M. Kugel, and A. Neumann, "Evaluation of Media Components and Process Parameters in a Sensitive and Robust Fed-Batch Syngas Fermentation System with Clostridium ljungdahlii," *Fermentation*, vol. 6, no. 2, p. 61, June 2020, doi: 10.3390/fermentation6020061.

[22] N. A. Istiqomah, G. M. Krista, R. Mukti, M. T. A. P. Kresnowati, and T. Setiadi, "Enhance the Growth of Clostridium ljungdahlii Microbial Cells by Modifying the Medium Composition and Trace Metals," *EC*, vol. 1, pp. 21–29, Jan. 2023, doi: 10.4028/p-t9r224.

[23] J. Jack, J. Lo, P.-C. Maness, and Z. J. Ren, "Directing Clostridium ljungdahlii fermentation products via hydrogen to carbon monoxide ratio in syngas," *Biomass and Bioenergy*, vol. 124, pp. 95–101, May 2019, doi: 10.1016/j.biombioe.2019.03.011.

[24] L. Perret, N. Boukis, and J. Sauer, "Synthesis gas fermentation at high cell density: How pH and hydrogen partial pressure affect productivity and product ratio in continuous fermentation," *Bioresource Technology*, vol. 391, p. 129894, Jan. 2024, doi: 10.1016/j.biortech.2023.129894.

[25] L. Perret, N. Boukis, and J. Sauer, "Influence of Increased Cell Densities on Product Ratio and Productivity in Syngas Fermentation," *Ind. Eng. Chem. Res.*, vol. 62, no. 35, pp. 13799–13810, Jan. 2023, doi: 10.1021/acs.iecr.3c01911.

[26] H. Younesi, G. Najafpour, and A. R. Mohamed, "Ethanol and acetate production from synthesis gas via fermentation processes using anaerobic bacterium, Clostridium ljungdahlii," *Biochemical Engineering Journal*, vol. 27, no. 2, pp. 110–119, Jan. 2005, doi: 10.1016/j.bej.2005.08.015.

[27] W. Van Hecke, R. Bockrath, and H. De Wever, "Effects of moderately elevated pressure on gas fermentation processes," *Bioresource Technology*, vol. 293, p. 122129, Dec. 2019, doi: 10.1016/j.biortech.2019.122129.

[28] R. L. Schmidt and C. L. Cooney, "PRODUCTION OF ACETIC ACID FROM HYDROGEN AND CARBON DIOXIDE BY CLOSTRIDIUM SPECIES ATCC 29797," *Chemical Engineering Communications*, vol. 45, no. 1–6, pp. 61–73, July 1986, doi: 10.1080/00986448608911372.

[29] J. L. Vega, E. C. Clausen, and J. L. Gaddy, "Study of gaseous substrate fermentations: Carbon monoxide conversion to acetate. 1. Batch culture," *Biotech & Bioengineering*, vol. 34, no. 6, pp. 774–784, Sept. 1989, doi: 10.1002/bit.260340607.

[30] M. Hermann *et al.*, "Electron availability in CO2 , CO and H2 mixtures constrains flux distribution, energy management and product formation in Clostridium ljungdahlii," *Microb Biotechnol*, vol. 13, no. 6, pp. 1831–1846, Jan. 2020, doi: 10.1111/1751-7915.13625.

[31] F. Oswald *et al.*, "Formic Acid Formation by Clostridium ljungdahlii at Elevated Pressures of Carbon Dioxide and Hydrogen," *Front. Bioeng. Biotechnol.*, vol. 6, p. 6, Feb. 2018, doi: 10.3389/fbioe.2018.00006.

[32] L. Puiman, E. Almeida Benalcázar, C. Picioreanu, H. J. Noorman, and C. Haringa, "Downscaling Industrial-Scale Syngas Fermentation to Simulate Frequent and Irregular Dissolved Gas Concentration Shocks," *Bioengineering*, vol. 10, no. 5, p. 518, Apr. 2023, doi: 10.3390/bioengineering10050518.

[33] G. Maschio, A. Lucchesi, and G. Stoppato, "Production of syngas from biomass," *Bioresource Technology*, vol. 48, no. 2, pp. 119–126, Jan. 1994, doi: 10.1016/0960-8524(94)90198-8.

[34] M. A. Bannoud, P. H. N. Ferreira, R. R. De Andrade, and C. A. M. Da Silva, "Control of an integrated first and second-generation continuous alcoholic fermentation process with cell recycling using model predictive control," *Chemical Engineering Communications*, vol. 212, no. 4, pp. 521–544, Apr. 2025, doi: 10.1080/00986445.2024.2417901.

[35] J. R. Phillips, K. T. Klasson, E. C. Clausen, and J. L. Gaddy, "Biological production of ethanol from coal synthesis gas: Medium development studies," *Appl Biochem Biotechnol*, vol. 39–40, no. 1, pp. 559–571, Sept. 1993, doi: 10.1007/BF02919018.

[36] C.-A. Aceves-Lara, E. Latrille, and J.-P. Steyer, "Optimal control of hydrogen production in a continuous anaerobic fermentation bioreactor," *International Journal of Hydrogen Energy*, vol. 35, no. 19, pp. 10710–10718, Oct. 2010, doi: 10.1016/j.ijhydene.2010.02.110.

[37] M. I. Sbarciog, S. Bhonsale, and J. Van Impe, “Observer-Based Predictive Control of a Continuous Co-Fermentation Process for Ethanol Production,” *Proceedings of FOODSIM 2020*, pp. 268–272, 2020.
[38] M. Srinivasarao, S. C. Patwardhan, and R. D. Gudi, “Nonlinear predictive control of irregularly sampled multirate systems using blackbox observers,” *Journal of Process Control*, vol. 17, no. 1, pp. 17–35, Jan. 2007, doi: 10.1016/j.jprocont.2006.08.007.
[39] L. Mears, S. M. Stocks, M. O. Albaek, G. Sin, and K. V. Gernaey, “Mechanistic Fermentation Models for Process Design, Monitoring, and Control,” *Trends in Biotechnology*, vol. 35, no. 10, pp. 914–924, Oct. 2017, doi: 10.1016/j.tibtech.2017.07.002.
[40] A. Caivano, W. Van Winden, G. Dragone, and S. I. Mussatto, “Enzyme-constrained metabolic model and in silico metabolic engineering of Clostridium ljungdahlii for the development of sustainable production processes,” *Computational and Structural Biotechnology Journal*, vol. 21, pp. 4634–4646, 2023, doi: 10.1016/j.csbj.2023.09.015.
[41] E. M. De Medeiros, J. A. Posada, H. Noorman, and R. M. Filhob, “Modeling and Multi-Objective Optimization of Syngas Fermentation in a Bubble Column Reactor,” in *Computer Aided Chemical Engineering*, vol. 46, Elsevier, 2019, pp. 1531–1536. doi: 10.1016/B978-0-12-818634-3.50256-3.
[42] J. K. Liu *et al.*, “Predicting proteome allocation, overflow metabolism, and metal requirements in a model acetogen,” *PLoS Comput Biol*, vol. 15, no. 3, p. e1006848, Mar. 2019, doi: 10.1371/journal.pcbi.1006848.
[43] M. Mohammadi, A. R. Mohamed, G. D. Najafpour, H. Younesi, and M. H. Uzir, “Kinetic studies on fermentative production of biofuel from synthesis gas using Clostridium ljungdahlii,” *ScientificWorldJournal*, vol. 2014, p. 910590, Jan. 2014, doi: 10.1155/2014/910590.
[44] G. Ruggiero, F. Lanzillo, F. Raganati, M. E. Russo, P. Salatino, and A. Marzocchella, “Bioreactor modelling for syngas fermentation: Kinetic characterization,” *Food and Bioproducts Processing*, vol. 134, pp. 1–18, July 2022, doi: 10.1016/j.fbp.2022.04.002.
[45] K. Valgepea *et al.*, “Arginine deiminase pathway provides ATP and boosts growth of the gas-fermenting acetogen Clostridium autoethanogenum,” *Metabolic Engineering*, vol. 41, pp. 202–211, May 2017, doi: 10.1016/j.ymben.2017.04.007.
[46] E. M. Medeiros, J. A. Posada, H. Noorman, and R. M. Filho, “Dynamic modeling of syngas fermentation in a continuous stirred-tank reactor: Multi-response parameter estimation and process optimization,” *Biotechnol Bioeng*, vol. 116, no. 10, pp. 2473–2487, Jan. 2019, doi: 10.1002/bit.27108.
[47] M. Zlokarnik, “Rührleistung in begasten Flüssigkeiten,” *Chemie Ingenieur Technik*, vol. 45, no. 9–10, pp. 689–692, May 1973, doi: 10.1002/cite.330450928.
[48] S. Ramió-Pujol, R. Ganigué, L. Bañeras, and J. Colprim, “Effect of ethanol and butanol on autotrophic growth of model homoacetogens,” *FEMS Microbiology Letters*, vol. 365, no. 10, May 2018, doi: 10.1093/femsle/fny084.
[49] H.-F. Zhu *et al.*, “Energy Conservation and Carbon Flux Distribution During Fermentation of CO or H2/CO2 by Clostridium ljungdahlii,” *Front. Microbiol.*, vol. 11, p. 416, Mar. 2020, doi: 10.3389/fmicb.2020.00416.
[50] I. K. Stoll, N. Boukis, and J. Sauer, “Syngas Fermentation at Elevated Pressure - Experimental Results,” ETA-Florence Renewable Energies, Jan. 2019. doi: 10.5071/27theubce2019-3cv.3.4.
[51] G. St-Pierre Lemieux, D. Groleau, and P. Proulx, “Introduction on Foam and its Impact in Bioreactors,” *Can J Biotech*, vol. 3, no. 2, pp. 143–157, Nov. 2019, doi: 10.24870/cjb.2019-000131.
[52] Z.-Y. Liu *et al.*, “Ethanol Metabolism Dynamics in Clostridium ljungdahlii Grown on Carbon Monoxide,” *Appl Environ Microbiol*, vol. 86, no. 14, pp. e00730-20, July 2020, doi: 10.1128/AEM.00730-20.
[53] H. Richter, B. Molitor, H. Wei, W. Chen, L. Aristilde, and L. T. Angenent, “Ethanol production in syngas-fermenting Clostridium ljungdahlii is controlled by thermodynamics rather than by

enzyme expression," *Energy Environ. Sci.*, vol. 9, no. 7, pp. 2392–2399, Jan. 2016, doi: 10.1039/C6EE01108J.
[54] M. Demler and D. Weuster-Botz, "Reaction engineering analysis of hydrogenotrophic production of acetic acid by *Acetobacterium woodii*," *Biotech & Bioengineering*, vol. 108, no. 2, pp. 470–474, Feb. 2011, doi: 10.1002/bit.22935.
[55] M. J. Mota, R. P. Lopes, I. Delgadillo, and J. A. Saraiva, "Microorganisms under high pressure — Adaptation, growth and biotechnological potential," *Biotechnology Advances*, vol. 31, no. 8, pp. 1426–1434, Dec. 2013, doi: 10.1016/j.biotechadv.2013.06.007.
[56] Y. Zhang *et al.*, "Critical impact of pressure regulation on carbon dioxide biosynthesis," *Bioresource Technology*, vol. 413, p. 131445, Dec. 2024, doi: 10.1016/j.biortech.2024.131445.
[57] V. Sivalingam, T. Haugen, A. Wentzel, and C. Dinamarca, "Effect of Elevated Hydrogen Partial Pressure on Mixed Culture Homoacetogenesis," *Chemical Engineering Science: X*, vol. 12, p. 100118, Nov. 2021, doi: 10.1016/j.cesx.2021.100118.
[58] N. Guan, J. Li, H. Shin, G. Du, J. Chen, and L. Liu, "Microbial response to environmental stresses: from fundamental mechanisms to practical applications," *Appl Microbiol Biotechnol*, vol. 101, no. 10, pp. 3991–4008, May 2017, doi: 10.1007/s00253-017-8264-y.
[59] J. Y. Oldshue, "Fluid Mixing in Fermentation Processes," in *Advances in Applied Microbiology*, vol. 2, Elsevier, 1960, pp. 275–287. doi: 10.1016/S0065-2164(08)70130-8.
[60] M. Douaire, J. Morchain, and A. Liné, "Mini review: relationship between hydrodynamic conditions and substrate influx toward cells," in *Proceedings of the 13th European Conference on Mixing*, 2009.
[61] R. Westlake, "Large-scale Continuous Production of Single Cell Protein," *Chemie Ingenieur Technik*, vol. 58, no. 12, pp. 934–937, Jan. 1986, doi: 10.1002/cite.330581203.
[62] N. A. Istiqomah, R. Mukti, M. T. A. P. Kresnowati, and T. Setiadi, "Modeling Syngas Fermentation for Ethanol Production under Fluctuating Inlet Gas Composition," *Bull. Chem. React. Eng. Catal.*, vol. 20, no. 2, pp. 331–345, Aug. 2025, doi: 10.9767/bcrec.20369.

Table of contents

Figures

Tables

Declaration of interests

☒ The authors declare that they have no known competing financial interests or personal relationships that could have appeared to influence the work reported in this paper.

☐ The authors declare the following financial interests/personal relationships which may be considered as potential competing interests: